Multi-wavelength generation in UV and green bands through SRS and parametric processes in silica fibers

Xiujuan Jiang, Qiang Fu, Lin Xu, Yuqiang Huang, Manjing Chen, Gholamreza Shayeganrad, Aurélien Coillet, Philippe Grelu, Timothy Lee

Multi-wavelength generation in UV and green bands through SRS and parametric processes in silica fibers

XIUJUAN JIANG[1,2,†,*], QIANG FU[2,†], LIN XU[2], YUQIANG HUANG[1], MANJING CHEN[1], GHOLAMREZA SHAYEGANRAD[2], AURÉLIEN COILLET[3], PHILIPPE GRELU[3], GILBERTO BRAMBILLA[2], AND TIMOTHY LEE[2]

[1] School of Electromechanical Engineering, Guangdong University of Technology, Guangzhou 510006, China
[2] Optoelectronics Research Centre, University of Southampton, Southampton SO17 1BJ, UK
[3] Laboratoire Interdisciplinaire Carnot de Bourgogne, Université de Bourgogne, 9 Avenue Alain Savary, F-21000, Dijon, France
[*] jiangxj@gdut.edu.cn

Compiled July 16, 2024

We report on multi-wavelength generation through simultaneous second-order and third-order nonlinear parametric processes following cascaded stimulated Raman scattering in silica fibers. The fiber system consists of a short standard step-index silica fiber and a microfiber tapered from it. When this system is pumped with a 130 ps laser at 1040 nm, multiple new wavelengths in the UV (340 nm-370 nm) and green (507 nm-547 nm) bands arise through four-wave mixing/sum-frequency generation from the pump and its Raman signals. The evolution of these wavelengths with increase of pump power is demonstrated in detail. Matching of frequencies and propagation constants in the involved processes are verified. This work provides a compact and simple method of multi-wavelength generation with fibers.

http://dx.doi.org/10.1364/ao.XX.XXXXXX

Nonlinear optical frequency conversion through parametric processes is an important way to obtain new wavelengths. The fiber-based four-wave mixing (FWM) governed by the third-order susceptibility $\chi^{(3)}$ has attracted much attention, of which the third-harmonic generation (THG) is a special case. A typical work was reported in 1983 [1]: an elliptical-core optical fiber was pumped by pulses at 1064 nm, and when two Stokes orders of stimulated Raman scattering (SRS) of the pump emerged, four combinations of the IR frequencies generated light within 355-385 nm by FWM, with anisotropic guiding structures playing a key role in phase matching. Afterwards, people have conducted experiments with various fibers and achieved signals in different spectral ranges, e.g., 355-430 nm in a nitrogen-doped silica fiber [2], visible generation in high-delta microstructured fibers [3], and 353 nm UV in a silica glass microfiber [4].

On the other hand, sum-frequency generation (SFG) is a nonlinear process governed by the second-order susceptibility $\chi^{(2)}$, of which the second-harmonic generation (SHG) is a special case. Although $\chi^{(2)}$ is supposed to vanish because of inversion symmetry of glass, the second-order processes did occur in silica fibers in practice, for example, in different experiments using microfibers [4, 5], which could be due to dipole from anisotropy at the core-cladding interface and higher order bulk nonlinear polarization quadrupolar terms [6]. Recently, the SHG efficiency was enhanced by transferring a crystalline GaSe coating onto a microfiber of phase-matching diameter [7].

Efforts to achieve multi-wavelength output in parametric processes have also been attempted, e.g. through frequencies mixing SHG with multiple CW sources [7], and THG with exposed- or suspended-core microstructured optical fibers [8, 9]. Multi-wavelength light sources are useful for various applications, e.g., multi-wavelength Raman spectroscopy is a powerful tool in identifying and quantifying the heterogeneous structure of materials [10]; use of multiple wavelengths can improve sensing accuracy, robustness and generalizability in optical pulse detection for unobtrusive physiological monitoring [11].

In this paper, we report on the experimental observation of multi-wavelength generation through optical frequency conversions governed by simultaneous $\chi^{(2)}$ and $\chi^{(3)}$ processes. It is built an all-fiber system that consists of a short conventional SMF-28 step-index silica fiber and a microfiber tapered from it. When this system is pumped with a single laser (130 ps @ 1040 nm), multiple new wavelengths in the UV band and the green band are detected. Analyses show that they could be explained by SRS of the pump and the ensuing FWM/SFG processes utilizing these additional pump frequencies. This work demonstrates a compact and straightforward method to realize multi-wavelength generation in a fully fiberized platform.

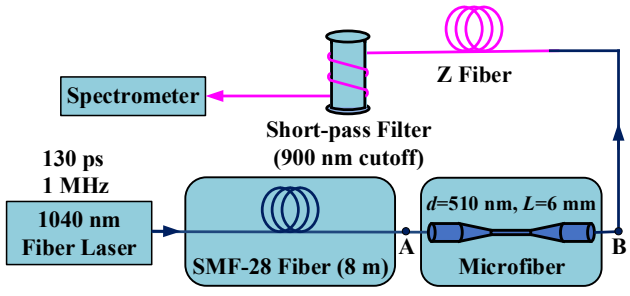

Fig. 1. Schematic of the experimental setup.

The experimental setup is shown in Fig. 1. The in-house built pump source is a fiber laser with 1040 nm wavelength, 130 ps pulse duration, 0.16 nm FWHM bandwidth and 1 MHz repetition rate [12]. The pump is coupled into a standard step-index silica fiber (SMF-28, Corning, $\sim$ 8 m). The microfiber is fabricated from the SMF-28 fiber on a tapering rig [13], and then removed from it and fixed in a protective plastic box. The microfiber reported in this paper has a waist diameter d= 510 nm and a waist length L= 6 mm. The untapered section of the SMF-28 fiber (about 75 cm) at the output end of microfiber is spliced to a pure silica core fiber with much lower UV absorption (Sumitomo, Z Fiber ITU-T G.654.C, $\sim$ 2 m). A segment of this Z fiber is wrapped around a rod to form a short-pass filter where bend loss attenuates the pump while transmitting the wavelengths shorter than about 900 nm. The output signals are detected with a spectrometer (OceanOptics, USB4000-UV-VIS). The spectrometer and the short-pass filter are connected with a patchcord with low UV transmission loss (OceanOptics, QP600-025-SR-BX, $\sim$ 20 cm). The pump spectrum is recorded with an optical spectrum analyzer (Yokogawa, AQ6370D), and its power is measured with a power meter.

In this setup, the pump at 1040 nm wavelength propagates in a multimoded regime along the SMF-28 fiber before it is coupled into the microfiber. The 8 m SMF-28 fiber is a preliminary nonlinear fiber giving significant SRS of the pump; the microfiber is the main nonlinear fiber, in which SRS of the pump is enhanced and the parametric processes occur, giving generation of multi-wavelength signals.

Figure 2(a) shows a typical output spectrum with distinct multi-wavelength signals in the UV and green bands. The highest average pump power used in the experiment is 415 mW, at which more peaks appear in both bands, see Fig. 2(b); here the continuum with wavelengths $\geq$ 800 nm is an artefact of the filter caused by considerable nonlinear pump broadening.

In order to make clear how the multiple wavelengths occur, Fig. 3 presents details of the pump spectra when its power ramps up, as well as the corresponding output signals (for clarity, the green and UV bands are given separately). The pump power P_0 is measured between the SMF-28 fiber and the microfiber, while P immediately after the microfiber. Each pump spectrum is normalized by its maximum, showing the relative intensities in dB of its spectral components. In the test, integration time of the OceanOptics spectrometer is adjusted adaptively to avoid signal saturation with pump power changing; the green and UV signal intensity counts for different cases in Fig. 3 are normalized by their integration time and thus comparable. Table 1 summarizes the signal wavelengths and their origins.

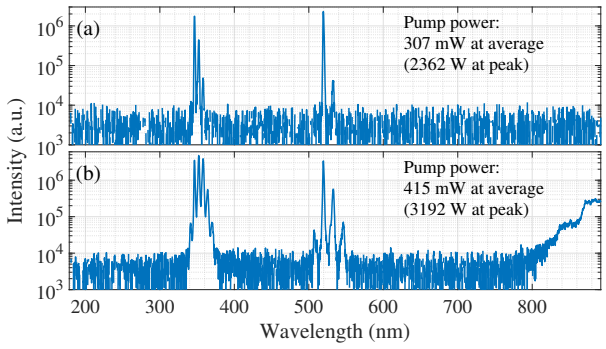

Fig. 2. Typical multi-wavelength output signals detected with the OceanOptics spectrometer.

Table 1. Summary of multi-wavelength signals observed in Fig. 3 and their origins.

Band	λ (nm)	Description
Pump	1040	λ_p (Pump wavelength)
	1090	λ_{S1} (First Stokes of Raman)
	1151	λ_{S2} (Second Stokes of Raman)
	990	λ_{aS} (Anti-Stokes of Raman)
Green	520	λ_{g1} (SFG: λ_p, λ_p)
	532	λ_{g2} (SFG: λ_p, λ_{S1})
	507	λ_{g3} (SFG: λ_p, λ_{aS})
	546	λ_{g4} (SFG: λ_p, λ_{S2} or λ_{S1}, λ_{S1})
UV	346	λ_{UV1} (FWM: λ_p, λ_p, λ_p)
	352	λ_{UV2} (FWM: λ_p, λ_p, λ_{S1})
	358	λ_{UV3} (FWM: λ_p, λ_{S1}, λ_{S1})
	364	λ_{UV4} (FWM: λ_{S1}, λ_{S1}, λ_{S1})
	341	λ_{UV5} (FWM: λ_p, λ_p, λ_{aS})
	370	λ_{UV6} (FWM: λ_{S1}, λ_{S1}, λ_{S2} or λ_p, λ_{S2}, λ_{S2})

In Fig. 3(a)-(d), at a low average pump power of 18 mW (138 W peak), neither the 8 m standard fiber nor the microfiber change the pump spectrum significantly, and only a signal at wavelength of $\sim$ 520 nm (λ_{g1}) is detected. This signal is the second harmonic of the 1040 nm pump (λ_p).

In Fig. 3(e)-(h), when the pump power is increased to 50 mW (385 W peak), the pump spectra remain similar and the 520 nm signal is stronger. A signal at $\sim$ 346 nm (λ_{UV1}) arises, and it is the third harmonic of the pump.

In Fig. 3(i)-(l), at a pump power of 200 mW (1538 W peak), both the 520 nm and 346 nm signals are stronger than the previous. The intense pump enhances nonlinear interactions in the standard fiber and in the microfiber, and thus a wavelength of $\sim$ 1090 nm (λ_{S1}) arises, which is the first Stokes SRS of the 1040 nm pump in a silica fiber. FWM from this signal and the pump generates another wavelength at $\sim$ 352 nm (λ_{UV2}).

In Fig. 3(m)-(p), with pump power of 307 mW (2362 W peak), the first Stokes SRS of the pump already occurs upon passing the standard fiber; further nonlinear interactions in the microfiber give rise to the anti-Stokes SRS at $\sim$ 990 nm (λ_{aS}) and the second Stokes SRS at $\sim$ 1150 nm (λ_{S2}). SFG from the 1040 nm pump and its first Stokes SRS at 1090 nm produces a new wavelength at $\sim$ 532 nm (λ_{g2}) in the green band, while FWM from them produces the 358 nm (λ_{UV3}) in the UV band.

In Fig. 3(q)-(t), when the average pump power reaches 415 mW (3192 W peak), two more wavelengths in the green band and three more wavelengths in the UV band are formed, see Table 1 for their origins.

Hence, through SRS and parametric processes in a standard fiber and a taper from it, the 1040 nm pump operating with average power $\sim$ 400 mW ($\sim$ 3000 W peak) stimulates three Raman peaks in its own band, generating four wavelengths spaced by $\sim$ 12 nm in the green band and six wavelengths spaced by $\sim$ 6 nm in the UV band. The spectral intervals for these frequency

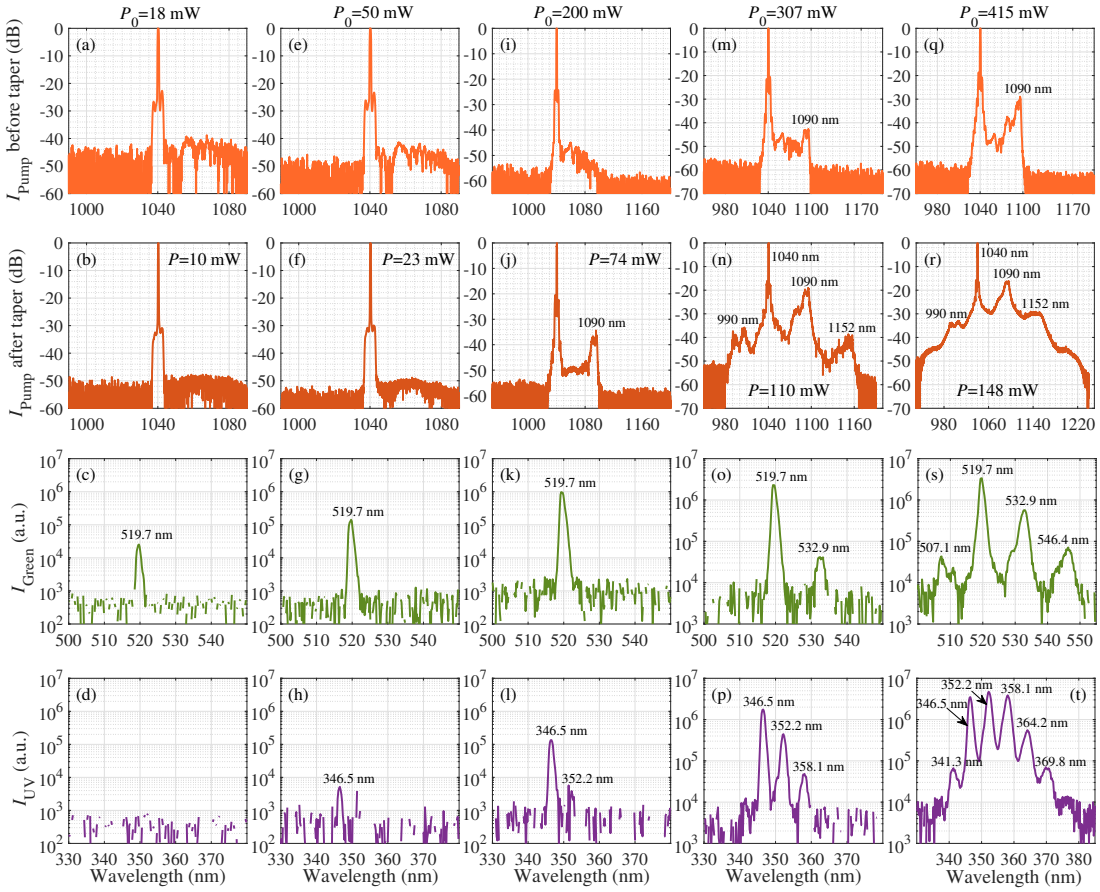

Fig. 3. Normalized pump spectra before (the 1st row) and after (the 2nd row) the microfiber at different pump power, and their corresponding green band (the 3rd row) and UV band (the 4th row) signals. (a)-(d) average pump power P_0=18 mW; (e)-(h) P_0=50 mW; (i)-(l) P_0=200 mW; (m)-(p) P_0=307 mW; (q)-(t) P_0=415 mW. (P_0 and P are respectively measured at points A and B in Fig. 1.)

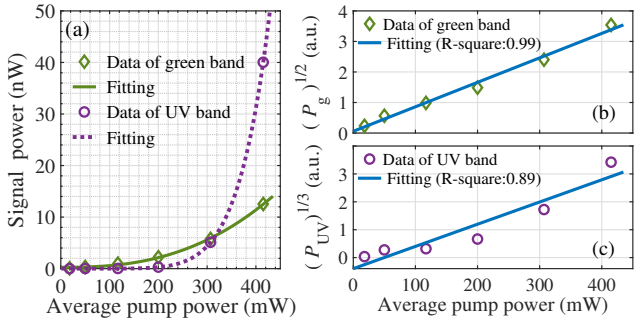

Fig. 4. (a) Signal power in green and UV bands vs. average pump power; (b) square root of power in green band and (c) cube root of power in UV band vs. average pump power.

mixed signals are in agreement with that expected for a ∼ 13 THz Raman frequency shift of silica fiber. This is an observation similar to that reported in [1], but only the third-order nonlinear interactions were involved in that early work.

To analyse the signal power trends, the green and UV bands are integrated over spectral ranges of 500-560 nm and 320-380 nm, respectively, and their powers are calibrated with a power meter (Thorlabs PM100D/S130VC). Figure 4(a) shows the green and UV powers against average pump power. Consistent with the results in Fig. 3, the green signal starts at a lower pump power, and remains stronger than the UV until the pump power ramps up to about 300 mW. The maximum green and UV powers are ∼ 13 nW and 40 nW, respectively, at average pump power of 415 mW. It should be noted that, because the microfiber is made from standard silica fiber of which wavelengths below ∼ 353 nm are not within the transmission range, the signals at 352 nm, 346 nm or 341 nm will experience more loss in the 75 cm output pigtail of the microfiber. So the actual total power of the UV band should be higher.

In Fig. 4(b), the square root of green power evolves linearly with the pump power, which is a clear signature of the second-order nonlinear interaction. In Fig. 4(c), the cube root of UV power basically agrees with the linear fit expected for the third-order nonlinear process; the small deviation may be due to pump-power-dependent SPM/XPM effects, as they could influence the phase matching and thus the energy conversion, and the UV loss mentioned above may be another reason. Such green/UV power dependence on pump power excludes the possibility that the detected SHG/THG lines might be false signals caused by the second-/third-order diffraction of the pump from the grating of the spectrometer, which is a linear process.

Significant FWM requires matching of the frequencies shown in Eq. 1 as well as matching of propagation constants (wave vectors) shown in Eq. 2, and the latter is referred to as phase matching. For SFG, the conditions are as in Eqs. 3 and 4.

$$\omega_1 + \omega_2 + \omega_3 = \omega_4, \quad \textbf{(1)}$$

Table 2. Selected phase matching cases for the SFG and FWM processes. PMD represents phase-matching diameter.

Input modes → Output mode	PMD (nm)
$HE_{11}(\lambda_p) + HE_{11}(\lambda_p) \rightarrow HE_{21}(\lambda_{g1})$	513
$HE_{11}(\lambda_p) + HE_{11}(\lambda_{S1}) \rightarrow HE_{21}(\lambda_{g2})$	526
$HE_{11}(\lambda_p) + HE_{11}(\lambda_{aS}) \rightarrow TM_{02}(\lambda_{g3})$	4515
$HE_{11}(\lambda_p) + HE_{11}(\lambda_{S2}) \rightarrow HE_{22}(\lambda_{g4})$	5002
$HE_{11}(\lambda_p) + HE_{11}(\lambda_p) + HE_{11}(\lambda_p) \rightarrow HE_{32}(\lambda_{UV1})$	1916
$HE_{11}(\lambda_p) + HE_{11}(\lambda_p) + HE_{11}(\lambda_{S1}) \rightarrow HE_{32}(\lambda_{UV2})$	1970
$HE_{11}(\lambda_p) + HE_{11}(\lambda_{S1}) + HE_{11}(\lambda_{S1}) \rightarrow HE_{12}(\lambda_{UV3})$	512
$HE_{11}(\lambda_{S1}) + HE_{11}(\lambda_{S1}) + HE_{11}(\lambda_{S1}) \rightarrow HE_{12}(\lambda_{UV4})$	521
$HE_{11}(\lambda_p) + HE_{11}(\lambda_p) + HE_{11}(\lambda_{aS}) \rightarrow HE_{32}(\lambda_{UV5})$	1859
$HE_{11}(\lambda_{S1}) + HE_{11}(\lambda_{S1}) + HE_{11}(\lambda_{S2}) \rightarrow HE_{12}(\lambda_{UV6})$	532

$$\beta_1 + \beta_2 + \beta_3 = \beta_4, \quad \textbf{(2)}$$

$$\omega_1 + \omega_2 = \omega_3, \quad \textbf{(3)}$$

$$\beta_1 + \beta_2 = \beta_3. \quad \textbf{(4)}$$

In Table 1, matching of the frequencies has already been verified. Intermodal phase matching can be achieved at proper fiber core diameters [4], depending on the specific wavelength combination and mode, and we check them in the involved parametric processes by solving the modal eigenvalue equations for a step index profile [14].

In our calculations, the light waves relating to the frequencies ω_j and propagation constants β_j on the left hand side of Eqs. 1-4 are referred to as input waves, while those on the right hand side as output waves. The actual phase matching would be complex, because each input wave would be in multiple transmission modes and thus there would be different combinations that could generate an output wave. We only consider the combinations in which all the input waves have the same modes and then obtain a part of the possible phase matching cases. Table 2 selects an instance from these cases for each green/UV signal listed in Table 1, by considering the modal overlaps between the signal and the pump [4, 15]. As the phase-matching diameters in Table 2 are all close to or larger than the 510 nm waist diameter, these signals would be generated in the taper transition regions. The continuum of diameters along these regions provides potential broadband frequency conversion.

The mechanism for $\chi^{(3)}$ in silica fiber is easy to understand. The $\chi^{(2)}$ processes can be attributed to glass-air surface dipole and bulk multipole of the microfiber [6], similar to [4, 5]. In our experiment, the pump is in multiple modes upon entering a microfiber with relatively long waist, giving considerable light energy escape from the core (Fig. 3 indicates more than 50% pump power loss in the microfiber). Such conditions enhance the surface nonlinearity at the core-cladding interface. In this work, the pump and green/UV signals are all in multiple modes; while lasers operating in a single mode are often desired, multi-mode sources would provide degrees of freedom in a variety of applications that are impossible in single-mode condition [16].

To conclude, we report on multi-wavelength generation through cascaded SRS and parametric processes (FWM and SFG) in a compact system consisting of an 8 m SMF-28 fiber and a microfiber (waist diameter d= 510 nm, length L= 6 mm) tapered from it. How the signals at these wavelengths occur with increase of pump power is demonstrated. Matching of frequencies as well as propagation constants in the involved processes are analysed and verified. Other than complex dual- or multi-pump structures, six wavelengths in the UV band (340-370 nm, spaced by 6 nm) and four wavelengths in the green band (507-547 nm, spaced by 12 nm) are generated with a single pump (130 ps @ 1040 nm) at 415 mW average power (3192 W peak). The transition regions of microfiber provide the necessary broadband frequency conversion.

For different needs, the output wavelengths could be altered flexibly by tuning the pump wavelength, while the number of output wavelengths can be controlled by adjusting the pump power. This work provides a proof of principle to realize multi-wavelength generation based on the simultaneous second-order and third-order nonlinear effects in fibers. The signal power and features can be improved by optimizing the preliminary fiber and microfiber parameters, and more progress will be reported separately.

Funding. National Natural Science Foundation of China (62275055); Natural Science Foundation of Guangdong Province (2019A1515011229); CSC (202008440059); EPSRC (EP/L01243X/1, EP/P030181/1); RS (IE131732).

Disclosures. The authors declare no conflicts of interest.

Data availability. Data underlying the results presented in this paper are not publicly available at this time but may be obtained from the authors on reasonable request.

REFERENCES

1. J. M. Gabriagues, Opt. Lett. **8**, 183 (1983).
2. I. A. Bufetov, M. V. Grekov, K. M. Golant, E. M. Dianov, and R. R. Khrapko, Opt. Lett. **22**, 1394 (1997).
3. A. Efimov, A. J. Taylor, F. G. Omenetto, J. C. Knight, W. J. Wadsworth, and P. St. J. Russell, Opt. Express **11**, 2567 (2003).
4. V. Grubsky and J. Feinberg, Opt. Commun. **274**, 447 (2007).
5. M. A. Gouveia, T. Lee, R. Ismaeel, M. Ding, N. G. R. Broderick, C. M. B. Cordeiro, and G. Brambilla, Appl. Phys. Lett. **102**, 201120 (2013).
6. R. W. Terhune and D. A. Weinberger, J. Opt. Soc. Am. B **4**, 661 (1987).
7. Z. Hao, B. Jiang, Y. Ma, R. Yi, X. Gan, and J. Zhao, Opto-Electron Adv. **6**, 230012 (2023).
8. S. C. Warren-Smith, K. Schaarschmidt, M. Chemnitz, E. P. Schartner, H. Schneidewind, H. Ebendorff-Heidepriem, and M. A. Schmidt, Opt. Lett. **44**, 626 (2019).
9. T. Cheng, X. Zhou, Y. Sun, X. Yan, X. Zhang, F. Wang, S. Li, T. Suzuki, and Y. Ohishi, Opt. Express **28**, 28750 (2020).
10. Z. Wu, Chinese J. Catal. **35**, 1591 (2014).
11. D. Ray, T. Collins, S. I. Woolley, and P. V. S. Ponnapalli, IEEE Reviews in Biomedical Engineering **16**, 136 (2023).
12. Y. Wu, Q. Fu, S. Liang, F. Poletti, D. J. Richardson, and L. Xu, Opt. Express **31**, 23419 (2023).
13. G. Brambilla, F. Xu, P. Horak, Y. Jung, F. Koizumi, N. P. Sessions, E. Koukharenko, X. Feng, G. S. Murugan, J. S. Wilkinson, and D. J. Richardson, Adv. Opt. Photon. **1**, 107 (2009).
14. A. Snyder and J. Love, *Optical Waveguide Theory*, 1st ed. (Springer, 1983),
15. J. Lægsgaard, J. Opt. Soc. Am. B **27**, 1317 (2010).
16. L. G. Wright, W. H. Renninger, D. N. Christodoulides, and F. W. Wise, Optica **9**, 824 (2022).

REFERENCES

1. J. M. Gabriagues, "Third-harmonic and three-wave sum-frequency light generation in an elliptical-core optical fiber," Opt. Lett. **8**(3), 183–185 (1983).
2. I. A. Bufetov, M. V. Grekov, K. M. Golant, E. M. Dianov, and R. R. Khrapko, "Ultraviolet-light generation in nitrogen-doped silica fiber," Opt. Lett. **22**(18), 1394–1396 (1997).
3. A. Efimov, A. J. Taylor, F. G. Omenetto, J. C. Knight, W. J. Wadsworth, and P. St. J. Russell, "Phase-matched third harmonic generation in microstructured fibers," Opt. Express **11**(20), 2567–2576 (2003).
4. V. Grubsky and J. Feinberg, "Phase-matched third-harmonic UV generation using low-order modes in a glass micro-fiber," Opt. Commun. **274**(2), 447–450 (2007).
5. M. A. Gouveia, T. Lee, R. Ismaeel, M. Ding, N. G. R. Broderick, C. M. B. Cordeiro, and G. Brambilla, "Second harmonic generation and enhancement in microfibers and loop resonators," Appl. Phys. Lett. **102**(20), 201120 (2013).
6. R. W. Terhune and D. A. Weinberger, "Second-harmonic generation in fibers," J. Opt. Soc. Am. B **4**(5), 661–674 (1987).
7. Z. Hao, B. Jiang, Y. Ma, R. Yi, X. Gan, and J. Zhao, "Broadband and continuous wave pumped second-harmonic generation from microfiber coated with layered GaSe crystal," Opto-Electron Adv. **6**(9), 230012 (2023).
8. S. C. Warren-Smith, K. Schaarschmidt, M. Chemnitz, E. P. Schartner, H. Schneidewind, H. Ebendorff-Heidepriem, and M. A. Schmidt, "Tunable multi-wavelength third-harmonic generation using exposed-core microstructured optical fiber," Opt. Lett. **44**(3), 626–629 (2019).
9. T. Cheng, X. Zhou, Y. Sun, X. Yan, X. Zhang, F. Wang, S. Li, T. Suzuki, and Y. Ohishi, "Supercontinuum-induced multi-wavelength third-harmonic generation in a suspended-core microstructured optical fiber," Opt. Express **28**(20), 28750–28761 (2020).
10. Z. Wu, "Multi-wavelength Raman spectroscopy study of supported vanadia catalysts: Structure identification and quantification," Chinese J. Catal. **35**(10), 1591–1608 (2014).
11. D. Ray, T. Collins, S. I. Woolley, and P. V. S. Ponnapalli, "A review of wearable multi-wavelength photoplethysmography," IEEE Reviews in Biomedical Engineering **16**, 136–151 (2023).
12. Y. Wu, Q. Fu, S. Liang, F. Poletti, D. J. Richardson, and L. Xu, "15-μJ picosecond hollow-core-fiber-feedback optical parametric oscillator," Opt. Express **31**(14), 23419–23429 (2023).
13. G. Brambilla, F. Xu, P. Horak, Y. Jung, F. Koizumi, N. P. Sessions, E. Koukharenko, X. Feng, G. S. Murugan, J. S. Wilkinson, and D. J. Richardson, "Optical fiber nanowires and microwires: fabrication and applications," Adv. Opt. Photon. **1**(1), 107–161 (2009).
14. A. Snyder and J. Love, *Optical Waveguide Theory*, 1st ed. (Springer, 1983), Chap. 11, pp218–219; Chap. 12, pp248–258.
15. J. Lægsgaard, "Theory of surface second-harmonic generation in silica nanowires," J. Opt. Soc. Am. B **27**(7), 1317–1324 (2010).
16. L. G. Wright, W. H. Renninger, D. N. Christodoulides, and F. W. Wise, "Nonlinear multimode photonics: nonlinear optics with many degrees of freedom," Optica **9**(7), 824–841 (2022).